LETTER • OPEN ACCESS

230 nm wavelength range far-UVC LED with low Al-composition differentiation between well and barrier layers of MQWs

Applied Physics Express 17, 042008 (2024) LETTER
https://doi.org/10.35848/1882-0786/ad3e48

230 nm wavelength range far-UVC LED with low Al-composition differentiation between well and barrier layers of MQWs

Kenjiro Uesugi[1,2], Ryota Akaike[1*], Shuhei Ichikawa[3,4], Takao Nakamura[5], Kazunobu Kojima[3], Masahiko Tsuchiya[6], and Hideto Miyake[5]

[1] Organization for Research Initiative and Promotion, Mie University, Tsu, Mie 514-8507, Japan
[2] Graduate School of Regional Innovation Studies, Mie University, Tsu, Mie 514-8507, Japan
[3] Graduate School of Engineering, Osaka University, Suita, Osaka 565-0871, Japan
[4] Research Center for Ultra-High Voltage Electron Microscopy, Ibaraki, Osaka 567-0047, Japan
[5] Graduate School of Engineering, Mie University, Tsu, Mie 514-8507, Japan
[6] Stanley Electric Co., Yokohama, Kanagawa 225-0014, Japan

*E-mail: akaike@elec.mie-u.ac.jp

Received January 23, 2024; revised April 1, 2024; accepted April 12, 2024; published online April 29, 2024

Reducing the average Al composition of $Al_xGa_{1-x}N/Al_yGa_{1-y}N$ multiple quantum wells (MQWs) is an effective approach to increase the current injection efficiencies of far-UV-C LEDs (far-UVC LEDs). A reduction can be realized by decreasing the Al-composition differentiation between the well and barrier layers. Compared to conventional MQWs, a 230 nm wavelength far-UVC LED equipped with a single-Al-composition and a 39 nm thick light-emitting layer exhibits a higher external quantum efficiency (EQE). The EQE of far-UVC LEDs with low Al-composition differentiation (~1%) is enhanced to approximately 0.6% and 1.4% under continuous wave operations at 230 nm and 236 nm wavelengths, respectively.

Supplementary material for this article is available online

Far-UV-C (far-UVC) light with wavelengths shorter than 240 nm can inactivate bacteria and viruses[1–5] without harming the human body.[6–9] Although excimer lamps with a 222 nm wavelength have practical applications, they are bulky, fragile, and only emit light with a specific wavelength. AlGaN-based LEDs have promise as an alternative in the far-UVC region. Several studies have realized high-efficiency far-UVC LEDs with external quantum efficiencies (EQEs) approaching 1% at wavelengths near 230 nm.[10–16] However, the efficiency and output power of far-UVC LEDs remain much lower than those of LEDs with longer wavelengths.[17–25]

This report examines the impact of the light-emitting layer structure on the EQE of far-UVC LEDs with a wavelength of around 230 nm. The EQE of an LED is the product of the radiative recombination efficiency (RRE) in the light-emitting layers, the current injection efficiency (CIE), and the light extraction efficiency (LEE). The design of the light-emitting layer and the electron-blocking layer (EBL) significantly affect the CIE of far-UVC LEDs. A higher offset energy in the conduction band adequately confines the electrons in the light-emitting layer, resulting in a high CIE. However, the ingenuity of the EBL design is limited for far-UVC LEDs because no III-nitride semiconductor has a larger bandgap energy than AlN. Another approach to improve CIE is to structurally modify the light-emitting layers. This includes increasing the volume, which is realized by incrementing the period of multiple quantum wells (MQWs)[14] or expanding the quantum well thickness. In addition, reducing the average Al composition of the light-emitting layer can enhance carrier confinement because the dominant factor in the emission wavelength is the Al composition of the well layer. Reducing the Al composition of the barrier layer can decrease the average Al composition of the MQWs while maintaining a fixed emission wavelength. However, reducing the Al composition of the barrier layer may have some drawbacks. For example, more minor compositional differences between the well and barrier layers weaken the confinement of carriers to the well layers. It has also been reported that a smaller Al composition difference between the well and barrier layers results in $\boldsymbol{E}//c$ polarization.[26] Consequently, lowering the Al composition of the barrier layer in MQWs does not necessarily enhance EQE as it should improve CIE but may lower RRE and LEE.

In this study, an extreme condition with a reduced Al composition in the barrier layer of MQWs showed that a higher EQE can be obtained when the Al composition of the well layer and barrier layer are identical. That is, an AlGaN film with a single-Al-composition and a 39 nm thick light-emitting layer displayed a higher EQE than that of a conventional $Al_xGa_{1-x}N/Al_yGa_{1-y}N$ MQW.

First, 600 nm thick low threading dislocation density (TDD) AlN templates were prepared on sapphire substrates by combining sputtering deposition of AlN and post-deposition high-temperature face-to-face annealing. The details are reported elsewhere.[27–29] The substrate temperature for sputtering, temperature set of the thermal cycle annealing,[30] and annealing duration were adjusted to 750 °C, 1600 °C–1680 °C, and 40 h, respectively. The density of the edge-type dislocation estimated by X-ray rocking curve measurements was $\sim 1 \times 10^8$ cm^{-2}. The screw- and mix-type dislocation densities were less than 1×10^5 cm^{-2} by counting the hillock density using the same technique described elsewhere.[25] Then the far-UVC LED structures were grown on the AlN templates with metalorganic vapor phase epitaxy (MOVPE) in the following order: 200 nm thick homoepitaxial AlN, 40 nm thick compositionally graded unintentionally doped (UID) AlGaN buffer, 1.0–1.7 μm thick $Al_{0.87}Ga_{0.13}N$:Si current-spreading layer, light-emitting layer, 10 nm thick UID-AlN EBL, 22 nm thick compositionally graded AlGaN:Mg p-type layer, and 200 nm thick GaN:Mg contact layer. Thick p-GaN was used to obtain better electric performance compared with p-AlGaN.

We prepared five samples with different light-emitting layer structures (Table I). Samples A and B consisted of 8 conventional pairs of $Al_xGa_{1-x}N/Al_yGa_{1-y}N$ MQW structures with a total thickness of ~39 nm and a peak emission wavelength (λ_p) around 230 nm. The Al compositions of the well layer (~2.0 nm thick) and barrier layers (~2.5 nm thick) were approximately 76%–77% and 86%. The emission wavelengths of these two samples were finitely (in the range of ~1 nm) varied by changing the ratio of the trimethylgallium supply for the well layers. Sample C, whose λ_p was 230 nm, was equipped with a 39 nm thick $Al_{0.80}Ga_{0.20}N$ single layer as its light-emitting layer. The light-emitting layers of Samples D (λ_p ~230 nm) and E (λ_p ~236 nm) were composed of 7 pairs of $Al_xGa_{1-x}N/Al_yGa_{1-y}N$ MQWs. However, the Al composition differentiation between the well and barrier layers in these two samples was as low as ~1%. All light-emitting layers (both well and barrier, in the case of MQWs) were Si-doped ($<5 \times 10^{17}$ cm^{-3}).

After epitaxial growth, 1 mm × 1 mm LED devices were fabricated on five samples. The n-type electrode was Ti/Al/Ni/Au formed on GaN:Si regrown on the n-AlGaN layer surface exposed with inductively coupled plasma reactive ion etching. The p-type electrode was Ni/Au. Both n and p-electrodes were annealed at 600 °C for 2 min (N_2 ambient) and at 550 °C for 5 min (O_2 ambient), respectively. Samples A, B, and C were characterized with on-wafer conditions to evaluate the impact of the light-emitting structure on the performance. Samples D and E were further processed and subsequently flip-chip mounted on AlN-based ceramic packages. The fabrication and characterization procedures of the packaged LEDs are reported elsewhere.[25] Encapsulation was not performed.

First, we evaluated the relationship between the light-emitting layer structure and the far-UVC LED performance. Because the luminescence wavelength greatly affects the optical properties of AlGaN in the far-UVC region, we paid attention to the emission wavelength distribution among the devices when evaluating their performances. Figures 1(a) and 1(b) compare the normalized electroluminescence (EL) spectra of samples A (with MQWs) and C (with a single layer AlGaN). Here, two devices with identical peak wavelengths were picked up. Both structures displayed a main emission peak from the light-emitting layer at a wavelength of ~230 nm and a broad peak at a wavelength of longer than 300 nm [Fig. 1(a)]. There is no relative intensity difference between the main emission and the long-wavelength luminescence. The long-wavelength luminescence intensity was about two orders of magnitude smaller than that of the main emission intensity. The broad, long wavelength luminescence may be photoluminescence generated by the excitation of the AlN template, which contained a high density of impurities such as oxygen and carbon,[31] due to the main emission at a wavelength of 230 nm. The spectral full width at half maximum was slightly smaller for Sample C (10.4 nm) than for Sample A (11.1 nm). The normalized spectra of the two samples agreed well at wavelengths longer than their peaks [Fig. 1(b)]. By contrast, Sample C showed a steeper decay in the intensity than Sample A at wavelengths shorter than the peaks. With a relatively low-Al composition single light-emitting layer, the self-absorption of shorter wavelength components than the peak wavelength can be enhanced within the light-emitting layer.

Figure 1(c) plots the current dependence of the peak wavelength for each sample. The emission wavelength blue-shifted with the injection current increment. This is partly attributed to the screening of the quantum confined Stark effect (QCSE). The change in the emission layer structure from the MQWs structure to the single layer structure should also drastically influence the significance of QCSE. However, the amount of blueshift was almost identical in the two samples. Therefore, the effect of QCSE may be quite small in these two samples.

Figure 2 compares the performances of Samples A, B, and C. Figure 2(a) is the EQE curve of the same LEDs shown in Fig. 1. Except for the low-current injection region (<10 mA), Sample C exhibited a higher EQE than Sample A [Fig. 2(a)]. The turn-on voltages of the two LEDs were 6 V, and the epitaxial structure of the light-emitting layer did not affect the operation voltage.

Figure 2(b) plots the relationship between EQE and the emission wavelength for several LEDs on each wafer. Samples A and B, which were equipped with almost the same MQWs light-emitting layer but slightly different quantum well Al compositions, demonstrated a clear wavelength dependence of EQE. The EQE decreased rapidly with a wavelength blueshift around 1 nm. Sample C, which had a single AlGaN light-emitting layer, exhibited the same tendency as Samples A and B except that the EQE of Sample C was higher than those of Samples A and B at all wavelengths.

Next, we considered the performances of packaged far-UVC LEDs. Figures 3(a) and 3(b) show the *I–L* characteristics and EQE curves of Sample D with a peak wavelength of 230 nm and Sample E with that of 236 nm. Table II summarizes the light output power and maximum EQE (EQE_{max}) for each sample and operating condition. The characteristics between continuous wave (CW) operation and pulsed operation differed drastically, indicating the characteristics deteriorated due to Joule heating in the high-injection region. The effect of Joule heating was more pronounced at shorter wavelengths. This issue may be resolved by reducing the operating voltage via the improvement of n-AlGaN conductivity and p-electrode contact resistance. We observed that the EQE_{max} under CW operation can be improved up to 0.82% at λ_p of 230 nm and 1.88% at λ_p of 236 nm, respectively, upon shrinking the chip size of the LED to 400 μm × 300 μm. It is suspected that shrinking the chip size enhances both light extraction via the side wall of the chip and thermal dissipation through the package.

Even when the Al composition difference between the well and the barrier layer of MQWs was minimal or non-existent,

Table I. Light-emitting layer structure.

Sample	Well layer Al composition/ thickness	Barrier layer Al composition/thickness
A	76%/2.0 nm	86%/2.5 nm
B	77%/2.0 nm	86%/2.5 nm
C	80%/39 nm	
D	79%/2.0 nm	80%/2.5 nm
E	73%/2.0 nm	74%/2.5 nm

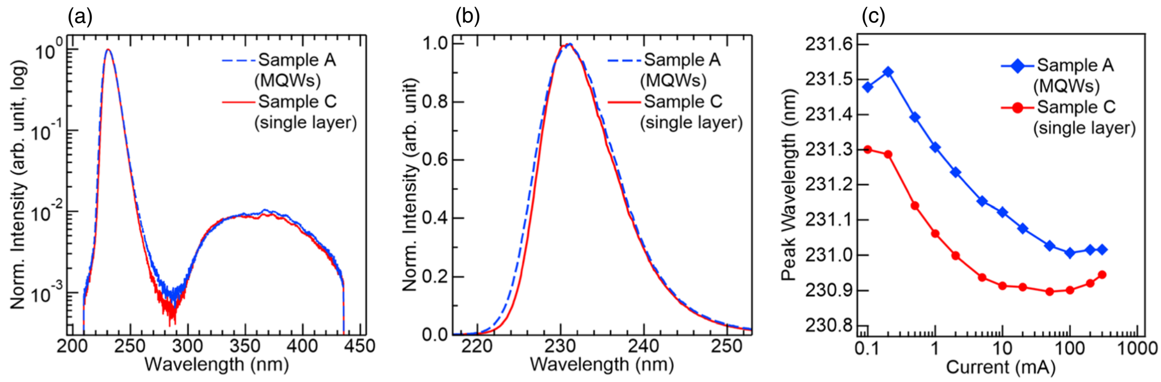

Fig. 1. EL spectra in (a) logarithmic scale and (b) linear scale for Sample A and Sample C. (c) Injection current dependence of the peak wavelength for Sample A and Sample C.

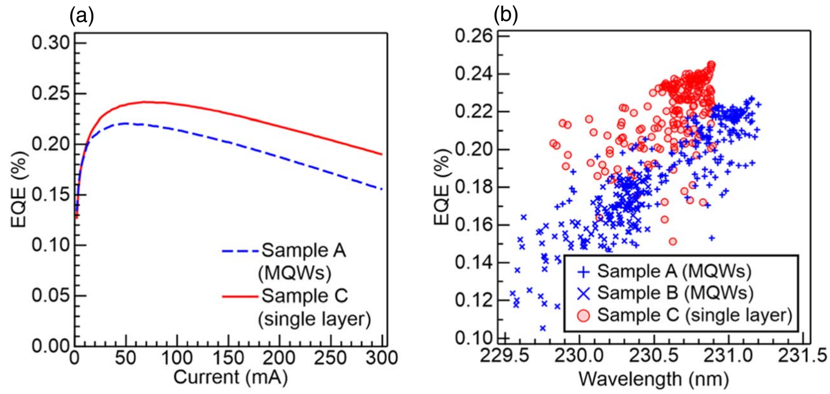

Fig. 2. (a) EQE curves of Samples A and C. (b) Relationship between EQE and the peak wavelength of far-UVC LEDs.

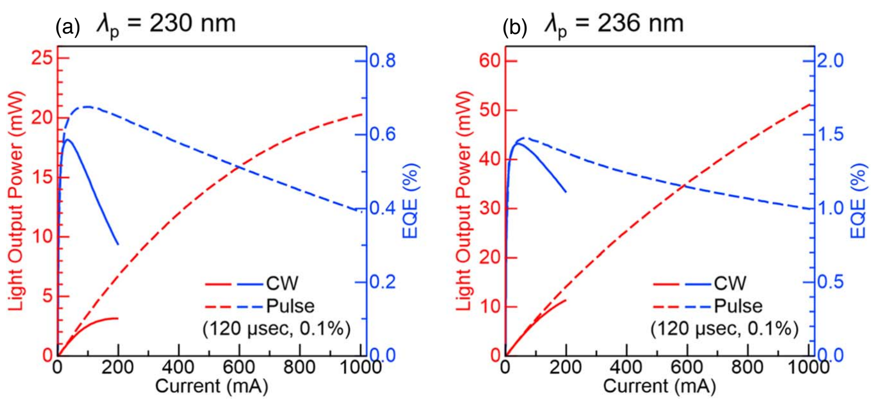

Fig. 3. *I–L* characteristics and EQE curves for (a) Sample D and (b) Sample E.

Table II. Performance of packaged far-UVC LEDs.

Peak wavelength	Output power CW (200 mA)/ pulse (1000 mA)	EQE_{max} CW/ pulse
230 nm (Sample D)	3.1 mW/20.3 mW	0.59%/0.68%
236 nm (Sample E)	11.4 mW/51.0 mW	1.44%/1.48%

the EQE of the light-emitting layer composed of a single Al composition AlGaN film was higher than that for conventional MQWs at the same emission wavelength. The improved EQE was attributed to the CIE improvement due to the reduced average Al composition of the light-emitting layer (simulation results of CIE are described in the supplementary material). It should be noted that the utilization of an AlGaN single layer instead of MQWs may have reduced RRE and promoted polarization switching,[26] thereby reducing LEE. Nevertheless, the single AlGaN light-emitting layer showed an improved EQE.

To investigate the influence on RRE, we performed cathodoluminescence (CL) mapping at room temperature for an AlGaN single layer without growing p-type conductive layers. (Photoluminescence measurements are also performed and the results are described in the supplementary material). Figures 4(a) and 4(b) show a CL intensity map for near band-edge emissions and a map of CL peak wavelengths reflecting Al compositions, respectively. The luminescence intensity distribution seemed to correspond to the in-plane inhomogeneity of the Al composition, which was derived from the peculiar surface morphology of AlGaN.[25] Carrier localization may have hindered capture by non-radiative

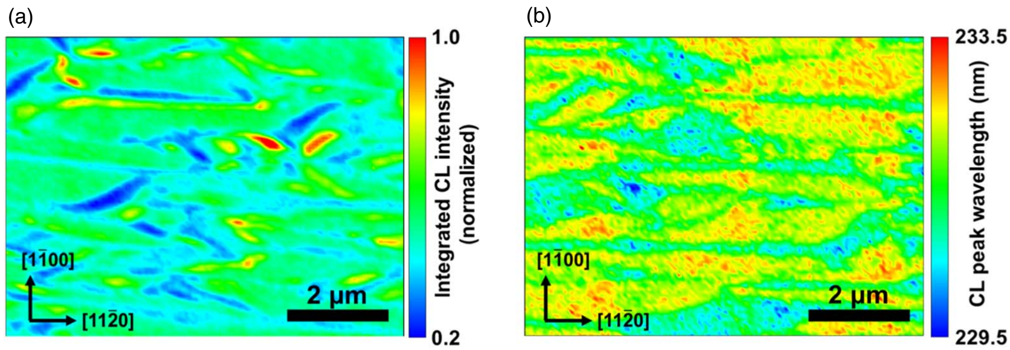

Fig. 4. (a) Integrated CL intensity map and (b) CL peak-wavelength map for near-band edge emissions in an AlGaN single layer.

recombination centers and suppressed the decrease in RRE. Further characterization will be discussed elsewhere. It has also been reported that in-plane compressive strain in the light-emitting layer prevents polarization switching.[26] The use of a high-temperature annealed AlN template with large compressive strain appeared to maintain $E \perp c$ polarization down to a short wavelength of 230 nm.[13]

In summary, LEDs with a single composition light-emitting layer, which measures several tens of nanometers thick, showed a high EQE. Since most existing III-nitride-based light-emitting devices employ MQWs structures, this study provides essential knowledge to design light-emitting devices in the far-UVC region.

Acknowledgments This work was partially supported by the New Energy and Industrial Technology Development Organization (NEDO) Intensive Support for Young Promising Researchers (No. 21502153-0), NEDO Leading Research Program, and the Japan Society for the Promotion of Science (JSPS) KAKENHI (Grant Nos. 21K14545 and 22H01970).

ORCID iDs Kenjiro Uesugi https://orcid.org/0000-0003-2605-5440 Ryota Akaike https://orcid.org/0000-0003-4410-1682 Shuhei Ichikawa https://orcid.org/0000-0001-7015-3748 Kazunobu Kojima https://orcid.org/0000-0003-0128-1978

1) M. Buonanno, B. Ponnaiya, D. Welch, M. Stanislauskas, G. Randers-Pehrson, L. Smilenov, F. D. Lowy, D. M. Owens, and D. J. Brenner, Radiat. Res. **187**, 493 (2017).
2) D. Welch, M. Buonanno, V. Grilj, I. Shuryak, C. Crickmore, A. W. Bigelow, G. Randers-Pehrson, G. W. Johnson, and D. J. Brenner, Sci. Rep. **8**, 2752 (2018).
3) K. Narita, K. Asano, K. Naito, H. Ohashi, M. Sasaki, Y. Morimoto, T. Igarashi, and A. Nakane, J. Hosp. Infect **105**, 459 (2020).
4) M. Buonanno, D. Welch, I. Shuryak, and D. J. Brenner, Sci. Rep. **10**, 10285 (2020).
5) H. Kitagawa, T. Nomura, T. Nazmul, K. Omori, N. Shigemoto, T. Sakaguchi, and H. Ohge, Am. J. Infect. Control **49**, 299 (2021).
6) T. Fukui et al., PLoS One **15**, e0235948 (2020).
7) J. Glaab et al., Sci. Rep. **11**, 14647 (2021).
8) T. Fukui et al., Photochem. Photobiol. **98**, 1365 (2022).
9) P. Zwicker et al., Sci. Rep. **12**, 2587 (2022).
10) A. Yoshikawa, R. Hasegawa, T. Morishita, K. Nagase, S. Yamada, J. Grandusky, J. Mann, A. Miller, and L. J. Schowalter, Appl. Phys. Express **13**, 022001 (2020).
11) N. L. Ploch, F. Mehnke, L. Sulmoni, H. K. Cho, M. Guttmann, J. Glaab, K. Hilbrich, T. Wernicke, S. Einfeldt, and M. Kneissl, Appl. Phys. Lett. **117**, 111102 (2020).
12) M. Jo, Y. Itokazu, and H. Hirayama, Appl. Phys. Lett. **120**, 211105 (2022).
13) A. Knauer et al., Appl. Phys. Lett. **122**, 011102 (2023).
14) H. Kobayashi, K. Sato, Y. Okuaki, T. Lee, T. Morishita, H. Goto, and N. Kuze, Appl. Phys. Lett. **112**, 101103 (2023).
15) T. Kolbe et al., Appl. Phys. Lett. **122**, 191101 (2023).
16) J. Rass, H. K. Cho, M. Guttmann, D. Prasai, J. Ruschel, T. Kolbe, and S. Einfeldt, Appl. Phys. Lett. **122**, 263508 (2023).
17) M. Shatalov et al., Appl. Phys. Express **5**, 082101 (2012).
18) J. R. Grandusky, J. Chen, S. R. Gibb, M. C. Mendrick, C. G. Moe, L. Rodak, G. A. Garrett, M. Wraback, and L. J. Schowalter, Appl. Phys. Express **6**, 032101 (2013).
19) M. Ichikawa, A. Fujioka, T. Kosugi, S. Endo, H. Sagawa, H. Tamaki, T. Mukai, M. Uomoto, and T. Shimatsu, Appl. Phys. Express **9**, 072101 (2016).
20) S. Nagai, K. Yamada, A. Hirano, M. Ippommatsu, M. Ito, N. Morishima, K. Aosaki, Y. Honda, H. Amano, and I. Akasaki, Jpn. J. Appl. Phys. **55**, 082101 (2016).
21) M. Kaneda, C. Pernot, Y. Nagasawa, A. Hirano, M. Ippommatsu, Y. Honda, H. Amano, and I. Akasaki, Jpn. J. Appl. Phys. **56**, 061002 (2017).
22) S. Inoue, N. Tamari, and M. Taniguchi, Appl. Phys. Lett. **10**, 141106 (2017).
23) T. Takano, T. Mino, J. Sakai, N. Noguchi, K. Tsubaki, and H. Hirayama, Appl. Phys. Express **10**, 031002 (2017).
24) Y. Matsukura, T. Inazu, C. Pernot, N. Shibata, M. Kushimoto, M. Deki, Y. Honda, and H. Amano, Appl. Phys. Express **14**, 084004 (2021).
25) K. Uesugi, S. Kuboya, K. Shojiki, S. Xiao, T. Nakamura, M. Kubo, and H. Miyake, Appl. Phys. Express **15**, 055501 (2022).
26) K. Kojima, A. A. Yamaguchi, M. Funato, Y. Kawakami, and S. Noda, J. Appl. Phys. **110**, 043115 (2011).
27) H. Miyake, C. H. Lin, K. Tokoro, and K. Hiramatsu, J. Cryst. Growth **155**, 456 (2016).
28) K. Uesugi, Y. Hayashi, K. Shojiki, and H. Miyake, Appl. Phys. Express **12**, 065501 (2019).
29) K. Uesugi and H. Miyake, Jpn. J. Appl. Phys. **60**, 120502 (2021).
30) D. Wang, K. Uesugi, S. Xiao, K. Norimatsu, and H. Miyake, Appl. Phys. Express **14**, 035505 (2021).
31) K. Shojiki, K. Uesugi, S. Kuboya, T. Inamori, S. Kawabata, and H. Miyake, Phys. Status Solidi b **258**, 2000352 (2021).